applied sciences

MDPI

Article

Effect of Nanohydroxyapatite on Silk Fibroin–Chitosan Interactions—Molecular Dynamics Study

Maciej Przybyłek [1,*], Anna Tuwalska [2], Damian Ledziński [3], Sandra Śmigiel [4], Alina Sionkowska [2], Iwona Białas [5] and Piotr Bełdowski [6]

[1] Department of Physical Chemistry, Pharmacy Faculty, Collegium Medicum of Bydgoszcz, Nicolaus Copernicus University in Toruń, 85096 Bydgoszcz, Poland
[2] Department of Biomaterials and Cosmetic Chemistry, Faculty of Chemistry, Nicolaus Copernicus University in Toruń, PL-87100 Toruń, Poland; planecka@doktorant.umk.pl (A.T.); as@chem.umk.pl (A.S.)
[3] Faculty of Telecommunications, Computer Science and Electrical Engineering, Bydgoszcz University of Science and Technology, PL-85796 Bydgoszcz, Poland; damian.ledzinski@pbs.edu.pl
[4] Faculty of Mechanical Engineering, Bydgoszcz University of Science and Technology, PL-85796 Bydgoszcz, Poland; sandra.smigiel@pbs.edu.pl
[5] CosmetoSAFE Consulting LLC, PL-05500 Piaseczno, Poland; i.bialas@cosmetosafe.pl
[6] International School of Bydgoszcz, Bośniacka 3, 85163 Bydgoszcz, Poland; piotr.beldowski.pb@gmail.com
* Correspondence: m.przybylek@cm.umk.pl

Abstract: Fibroin–chitosan composites, especially those containing nanohydroxyapatite, show potential for bone tissue regeneration. The physicochemical properties of these biocomposites depend on the compatibility between their components. In this study, the intermolecular interactions of fibroin and chitosan were analyzed using a molecular dynamics approach. Two types of systems were investigated: one containing acetic acid and the other containing calcium (Ca^{2+}) and hydrogen phosphate (HPO_4^{2-}) ions mimicking hydroxyapatite conditions. After obtaining the optimal equilibrium structures, the distributions of several types of interactions, including hydrogen bonds, ionic contacts, and hydrophobic contacts, along with structural and energetical features, were examined. The calculated binding energy values for the fibroin–chitosan complexes confirm their remarkable stability. The high affinity of fibroin for chitosan can be explained by the formation of a dense network of interactions between the considered biopolymers. These interactions were found to primarily be hydrogen bonds and ionic contacts involving ALA, ARG, ASN, ASP, GLN, GLU, GLY, LEU, PRO, SER, THR, TYR, and VAL residues. As established, the complexation of fibroin with chitosan maintains the β-sheet conformation of the peptide. β-Sheet fragments in fibroin are involved in the formation of a significant number of hydrogen bonds and ionic contacts with chitosan.

Keywords: biomaterials; chitosan; silk fibroin; molecular dynamics; intermolecular interactions; hydrogen bonds

Citation: Przybyłek, M.; Tuwalska, A.; Ledziński, D.; Śmigiel, S.; Sionkowska, A.; Białas, I.; Bełdowski, P. Effect of Nanohydroxyapatite on Silk Fibroin–Chitosan Interactions—Molecular Dynamics Study. *Appl. Sci.* **2024**, *14*, 4131. https://doi.org/10.3390/app14104131

Academic Editor: Alejandro Rodríguez Pascual

Received: 31 March 2024
Revised: 7 May 2024
Accepted: 10 May 2024
Published: 13 May 2024

1. Introduction

It is widely recognized that the interactions between proteins and polysaccharides are pivotal in both living organisms [1] and the development of novel biomaterials [2]. Among the polysaccharide analogues, proteoglycans deserve special attention. These biomolecules are composed of protein and glycosaminoglycan (GAG) moieties bound to the protein by the serine and threonine fragments [3]. They are typically found on the cell surface and in the extracellular matrix (ECM). Proteoglycans are essential for the strength and flexibility of cartilage and tendons. The absence of proteoglycans is associated with heart and respiratory failure, defects in skeletal development, and increased tumor metastasis [4].

Silk threads are considered to be one of the strongest natural fibers. They exhibit a high tensile strength of 4.8 GPa, very good flexibility [5–7] and high thermal stability [8–10]. Silk is more resistant to loads than Kevlar (the most potent manufactured fiber to date) [7,11,12].

Spiderweb silk exhibits exceptional mechanical properties [10,13]. However, silk produced on an industrial scale is primarily sourced from domesticated mulberry silkworms (*B. mori*) due to their ease of cultivation and higher thread yield from their cocoons compared to spider webs [10,13]. Natural silk thread is composed of two tightly packed bundles of fibroin fibers, glued with a sericin sheath and soluble in hot water. Fibroin protein is a dominant component of raw silk, accounting for 70%–80% of its weight [14–16]. The other components are sericin, wax, fats, and dyes [12,17]. Fibroin, has a high content of amino acids, with serine comprising approximately 12% [18], whereas collagen contains four times less amino acids [19]. The repetitive sequence of amino acids (alanine and glycine) already in the primary structure makes silk fibroin a highly ordered protein. An essential repeating motif of the fibroin amino acid sequence is $-(GLY\text{-}SER\text{-}GLY\text{-}ALA\text{-}GLY\text{-}ALA)_n$. These chains, connected by hydrogen bonds, form the antiparallel β-sheet structure. Due to the periodic primary structure, there are glycine residues in the secondary structure on one side of the surface of the β-sheet, interacting with the glycine residues of the adjacent chain. Similarly, on the other side of the surface of the β-sheet, there are serine and alanine residues interacting with similar residues of another neighboring chain (Figure 1). This quasi-crystalline structure is interrupted by stretches of the sequence containing other amino acids (e.g., TYR, ASP, ARG and VAL).

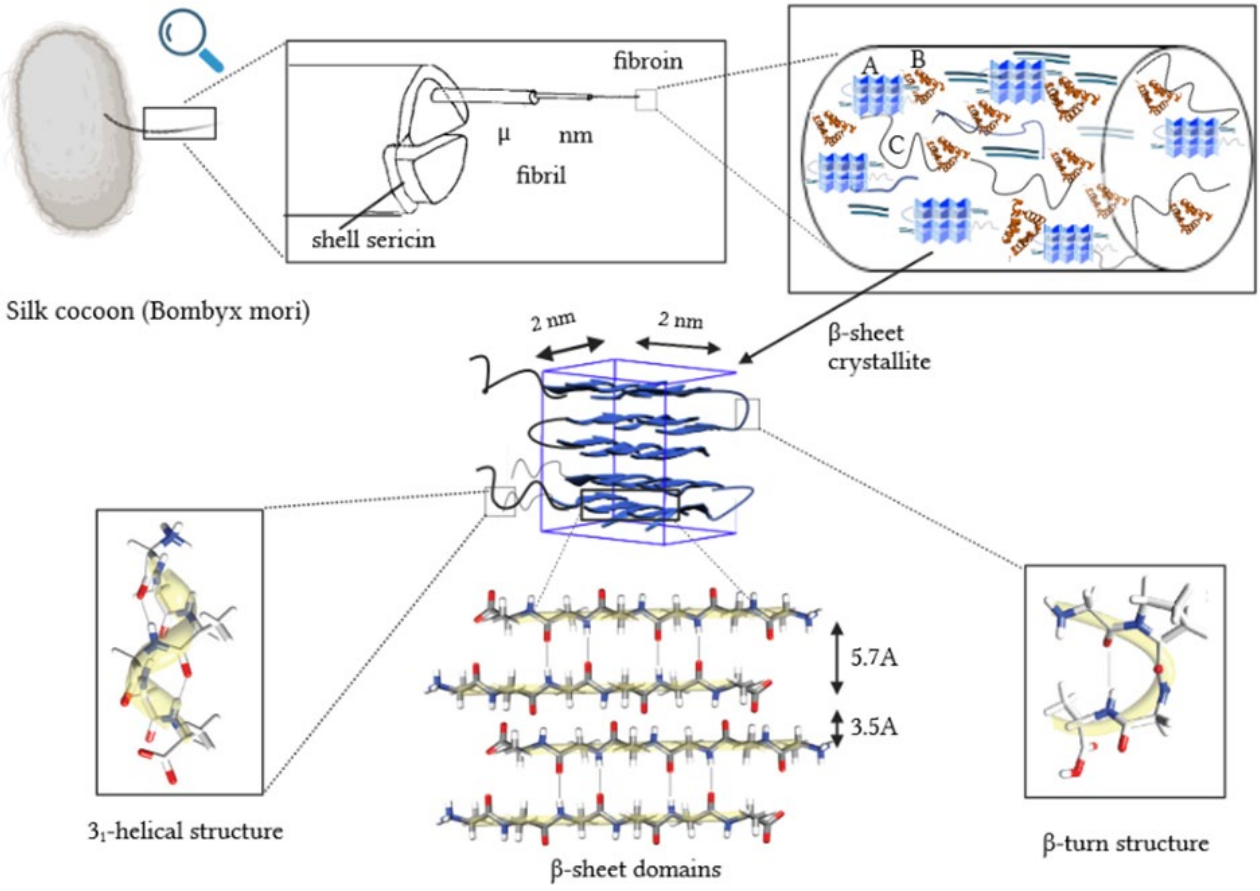

Figure 1. Silk thread morphology, based on [10,20–22]. The letters A, B and C denote crystalline region, α-helix structure and non-oriented amorphous area, respectively.

Silk fibers with a high proportion of regular glycine–alanine fragments tend to be more flexible due to weak interactions between chains in the β-sheet structure, but less stretchable as the polypeptide chains are under significant tension in this secondary structure. Fiber properties such as gloss and softness depend on differences in the size and characteristics of amino acid residues within irregular structural fragments. Crystalline regions within

fibers, marked as A in Figure 1, consist of tightly packed motifs of the antiparallel β-sheet, aligned along the fiber axis. Dispersion angle measurements revealed the presence of crystallites with dimensions of 2 × 2 × 2 nm [20]. However, these dimensions increase to 5–7 nm in length at slower reeling speeds [23]. Additionally, the analysis identified non-crystalline regions with two distinct morphologies: (i) oriented regions with an α-helix structure (B, Figure 1) and (ii) non-oriented amorphous areas (C, Figure 1). A closer insight into the less-ordered regions aligned with the fiber axis reveals the presence of the 3_1-helix motif (which grants elasticity to the fibers) and a greater abundance of β-bends/turns and potentially β-spirals. These β-structures, prevalent in spider silk, might be responsible for the rapid shrinking of the thread in water (super contraction effect) [24–26].

Silk fibroin consists of two main chains: a heavier H-chain (around 300 kDa in *B. mori*) with a hydrophobic nature and a lighter L-chain (25 kDa) with a hydrophilic nature. These chains are linked by a disulfide bridge. The structure also includes a chaperone protein, P25, which is a fibrohexamer glycoprotein. The structure of the silk thread is supported by strong hydrogen bonds, especially in the crystalline areas, and by Van der Waals interactions. According to Kaplan models, the primary structure's chain is predominantly hydrophobic, interspersed with small repetitive sections of a hydrophilic nature [27]. These alternating hydrophilic and hydrophobic interactions lead to the formation of micelles, where water is bound within the hydrophilic domains (approximately 8%). These micelles, measuring up to 200 nm in size, ultimately form fibroin globulins. When subjected to various physical or chemical stimuli, such as changes in pH, temperature fluctuations, variations in metal ion concentration, increased fibroin concentration, ultrasound exposure, or mechanical shearing, disordered and β-helical regions transform into ordered β-sheet structures. Concentrated globulins transition into a liquid crystal phase, with particles aligning parallel to one another as they flow, solidifying upon exposure to air to form a thread.

Due to its hydrophobic nature, and the presence of inter- and intramolecular strong hydrogen bonds in many crystalline regions, natural silk fibers dissolve only in a few solvents, including concentrated acids: H_3PO_4, HCOOH, H_3SO_4, and HCl and aqueous solutions of concentrated salts: LiSCN, LiBr, $CaCl_2$, $Ca(SCN)_2$, $ZnCl_2$, NH_4SCN, CuSO4, $Ca(NO_3)_2$ [17]. Despite the solubility limitation, it is possible to obtain many different forms of silk material, e.g., films, foams, hydrogels, powders, nanofibers, and microcapsules [18]. Silk is used not only in the clothing industry for producing fabrics, anti-allergic bedding, bulletproof vests, ropes, and parachutes, but also in medical applications. Silk fibers (catgut) have been used as surgical threads for years. There is a lot of interest in an aqueous solution of silk fibroin, which, thanks to its biocompatibility, biodegradability, and similarity to collagen and elastin, is successfully used in tissue engineering. Silk fibroin is a promising scaffold material for cell growth and regeneration in various damaged tissues, including connective, nervous, cartilage, and bone tissues [7]. Furthermore, it has a wide range of other biomedical and pharmaceutical applications, including drug carriers [28–30] and hydrogels for transparent wound dressings [31,32]. Notably, additional beneficial properties, such as antibacterial properties, increased strength, resistance to degradation, viscosity suitable for bioprinting, and others, can be achieved by adding other polymers, such as chitosan, hyaluronic acid, cellulose, sodium alginate, starch, carrageenan, collagen, gelatin, PVA, PVP, and poly(lactic acid) [33,34].

Among polysaccharide analogues, chitosan demonstrates exceptional biocompatibility and biodegradability [35,36]. It is derived from chitin, an abundant and renewable resource, and is widely acknowledged for its safety profile [36]. Its versatility and potential or actual applications have been widely demonstrated in numerous fields, including agriculture [37,38], pharmacy and medicine [30,36,37,39–43], food industry [36,37,44], textile industry [36,37,45,46], biotechnology [47], cosmetics [37,48–51], paper production [37,52] and various green and sustainable technologies [53–55]. Chitosan emerges as a highly desirable substance, owing to its non-toxicity, cationic nature, biocompatibility, and antibacterial properties, alongside its unique chemical composition [35].

In general, composites stabilized by strong intermolecular interactions exhibit superior mechanical durability. For instance, there are documented correlations between the denaturation temperature characterizing the thermal stability of protein-containing biomaterials and their mechanical and rheological properties [56–58]. Importantly, the direct evidence of the relationships between the strength and mechanical properties of intermolecular interactions was demonstrated by studies that explored experimental analysis with molecular dynamics computations [59,60]. Our previous research employed molecular dynamics simulations to explore complexes of chitosan/chitin with collagen [61–63] and hyaluronan [64]. Understanding these interactions is crucial for developing strategies for cartilage regeneration [65]. Likewise, chitosan–fibroin composites are relevant from biomedical and pharmaceutical perspectives [34,66–70]. Notably, chitosan/fibroin composites containing hydroxyapatite exhibit exceptional tissue regeneration potential due to their unique properties [66,68]. These composites hold promise for various applications. For instance, they could serve as durable, natural fillings and dental implant scaffolds. Notably, all the named substances—chitosan, fibroin, and hydroxyapatite—are either applied or considered as promising materials in dentistry thanks to their biocompatibility and mechanical properties [71–75]. Their degradation products are non-toxic, and the materials can be engineered to resist wear and tear depending on the number of intermolecular contacts stabilizing the molecular assemblies. Additionally, these composites can be used for bone reconstruction. The intermolecular contacts between silk fibroin and chitosan seems to be a key factor influencing the mechanical behavior of load-bearing applications [34,76]. A thorough understanding of these interactions will allow for the design of materials with controlled degradation rates. This could be crucial for creating scaffolds that degrade at a pace matching new bone tissue regeneration, thereby preventing the formation of pseudoarthrosis (a common complication in long bone defects characterized by improper mineralization) [77]. This study focuses on unraveling the intermolecular interactions between fibroin and chitosan in the presence of HPO_4^{2-} and Ca^{2+} ions using molecular dynamics simulations. The main goal is to elucidate the factors that contribute to the remarkable stability of these composites.

2. Methods

All molecular dynamics computations were carried out using an YASARA software [78,79], a comprehensive and versatile tool for modeling biopolymer complexes, including polysaccharide/peptide systems [61–64,80–82]. The structure of the chitosan was taken from PubChem (PubChem CID: 129662530) and modified to obtain polymer of total mass of 200 kDa (1250 monomer units). The deacetylation degree of the chitosan applied in this study was 100%. Notably, chitosan with a high degree of deacetylation is commonly used in fibroin composites [83–87]. A high degree of deacetylation results in a higher number of protonated amino groups in aqueous solutions, thus enhancing solubility and biocompatibility [88]. The structure of the silk fibroin heavy chain was obtained from https://alphafold.ebi.ac.uk/entry/B0FRJ4 accessed on 6 May 2024 (fibroin heavy chain Fib-h). In order to optimize the structure further, it was equilibrated for 5 ns. Additionally, a single chitosan chain was included in the simulation box, and five separate simulations, each lasting 40 ns, were conducted. Finally, 8 fibroin chains were added to chitosan for each system. Two cases have been studied: (1) with the presence of Ca^{2+} and HPO_4^{2-} ions (HPO_4^{2-}/Ca^{2+}) and (2) with the presence of acetic acid. Point charges for silk fibroin atoms were assigned using the AMBER14 force field [89], while charges for chitosan atoms were assigned using the GLYCAM06 force field [90]. Notably, studies employing the AMBER14 force field in peptide simulations frequently yielded results aligned with experimental observations [91–93]. This force field was modified compared to previous versions to better reproduce structural data obtained from NMR measurements [94]. The GLYCAM06 force field, utilized in this study alongside AMBER14, has shown a good quality of prediction of structural features in polysaccharides [95,96].

In the subsequent step, all molecular systems were used for the molecular dynamics computations. The applied approach included the water solvation effects and acid–base characteristics. For this reason, the procedure encompassed the adjustment of the structural features of hydrogen bonds to achieve appropriate protonation microstates of the peptide at pH = 7.0 [97]. The neutral pH was set for all systems considered in the study. The charge of the generated structures used for molecular dynamics simulations was set to zero. After equilibration and energy minimization, molecular dynamics (MD) simulations were run for 1 nanosecond. The simulations employed appropriate force fields for all atoms in the studied molecular systems: AMBER14 for fibroin, GLYCAM06 for chitosan, and TIP3P for water. Standard AMBER settings were used, including a 1.0 nm van der Waals cutoff and the Particle Mesh Ewald algorithm [98] for calculating electrostatic interactions. The equations of motion were integrated using time steps of 1.25 femtoseconds and 2.5 femtoseconds for bonded and non-bonded interactions, respectively, under the conditions of temperature (T) set at 310 K and pressure (P) at 101,325 Pa within the NPT ensemble [98]. The Berendsen barostat and thermostat [99], featuring a relaxation time of 1 fs, were employed to ensure constant pressure and temperature. To mitigate the impact of rescaling, YASARA avoids utilizing the highly variable instantaneous microscopic temperature and pressure for velocity rescaling in each simulation step (a characteristic of the classic Berendsen thermostat). Instead, it computes the scaling factor based on Berendsen's formula using the time-averaged temperature. The simulation duration time was set to 200 ns to ensure sufficient information for subsequent analysis. Achieving the optimal structure of the complex was confirmed based on several structural parameters, including the RMSD of the evolution of all atoms, radius gyration, and numbers of intermolecular interactions (Supplementary Figures S1 and S2). In order to determine binding energy and other critical characteristics, 1500 data points were meticulously chosen from the 50–200 ns timeframe, subsequent to the root mean square deviation/displacement (RMSD) analysis.

3. Results and Discussion

This study examined two chitosan–silk fibroin complexes. One complex incorporated Ca^{2+} ions and $HPO_4{}^{2-}$ to mimic nanohydroxyapatite, while the other contained acetic acid. The selection of the acetic acid environment as a reference simulation condition was guided by two considerations: its well-documented role as a stabilizer for fibroin [67] and its ability to dissolve both fibroin and chitosan [67,100]. The exemplary optimized structures of chitosan–silk fibroin complexes are presented in Figure 2. The detailed structural and geometric parameters, including hydrogen bond lengths, interaction distances, and binding energies, are provided in the Supplementary Materials. The analysis of the optimized structures revealed that basic amino groups in chitosan undergo protonation under all considered conditions. The role of charged ions in stabilizing these large biomolecular systems presents an intriguing aspect for investigation. Although the individual components of these complexes carry charges, the overall molecular assemblies themselves remain neutral due to the presence of counterions (CH_3COO^-, $HPO_4{}^{2-}$, Ca^{2+}). Molecular dynamics simulations unveil that the formation of complexes with both CH_3COOH and $HPO_4{}^{2-}/Ca^{2+}$ is energetically advantageous. However, the total binding energy, encompassing all stabilizing interactions, slightly favors the former system (7452 $\pm$ 397 kJ/mol) over the latter (6483 $\pm$ 561 kJ/mol). Despite these disparities, both values are remarkably high. Notably, the binding energies, calculated through similar procedures for chitosan-collagen complexes as reported in our previous studies [61,63], did not exceed 850 kJ/mol. This suggests a significantly lower mutual affinity between chitosan and collagen compared to chitosan-fibroin systems. Notably, fibroin is known to form semi-interpenetrating polymer network (semi-IPN) arrangements with chitosan [101]. Moreover, thermal studies have shown high compatibility and thermal stability of the chitosan-fibroin mixture [102].

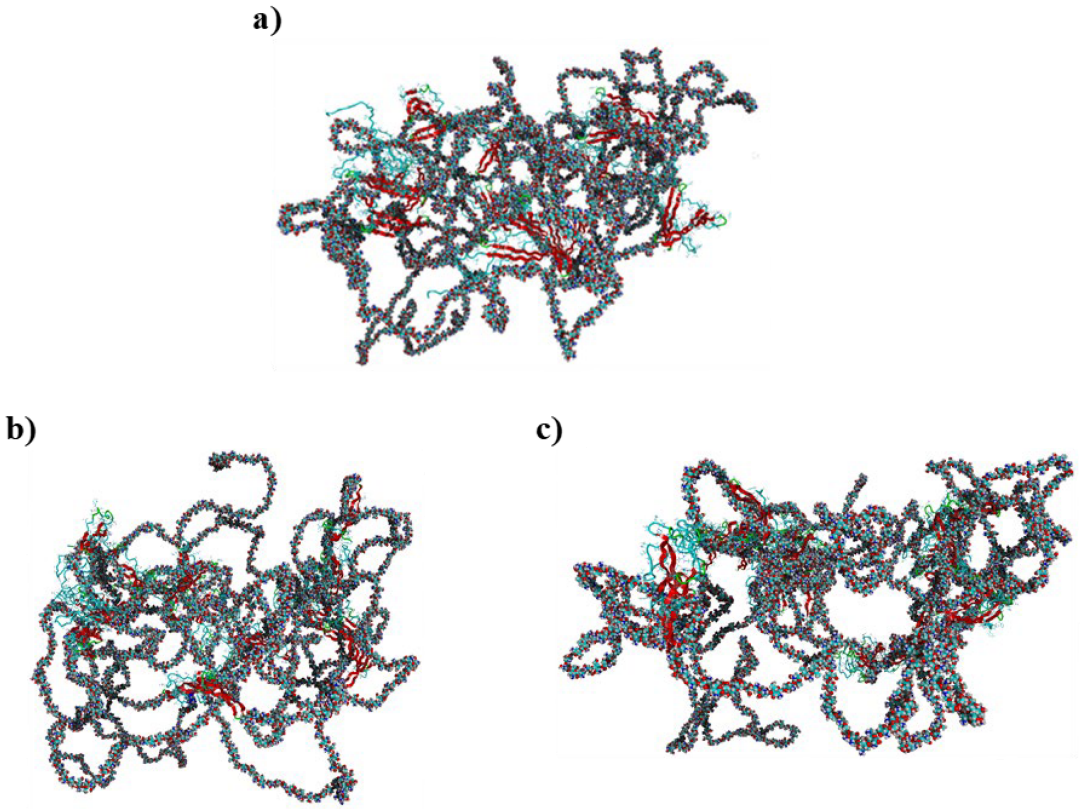

Figure 2. Visualization of the initial chitosan–silk fibroin structure (**a**) and the optimized complexes containing CH_3COOH (**b**) and HPO_4^{2-}/Ca^{2+} (**c**). Chitosan is presented in a ball model, while fibroin is in ribbon like structure. Fibroin helices are presented as solid turquoise lines, whereas chitosan is represented by a ball–stick model with colors representing the following elements: carbon—turquoise, nitrogen—dark blue, oxygen—red, and hydrogen–white.

Similar to chitosan, fibroin undergoes protonation in acidic conditions [103,104], as evidenced by computational results. While both biomolecules become positively charged through protonation, the formation of stable complexes is possible due to the presence of oppositely charged ions that neutralize the positive charge. Our previous studies [63] have demonstrated similar behavior in the case of collagen–chitosan systems. Importantly, both chitosan and proteins, such as collagen and fibroin, exhibit polyelectrolytic properties [105–107], leading to charge migration within the polymer chain and fluctuations in charge density within the biomolecule. These properties can be manifested in complex molecular systems. Nevertheless, similar calculations performed in previous studies [63] have shown that even oligomeric chitosan chains exhibit polyelectrolytic features. Since polyelectrolytes contain many ionic and polar groups, they are capable of forming various intermolecular contacts. Remarkably, the complexes investigated in this study reveal a dense network of interactions between chitosan and fibroin. The YASARA program (2021) employed in this study was capable of identifying various primary types of interactions in the considered fibroin–chitosan complexes, such as ionic contacts, hydrogen bonds, and hydrophobic interactions. Of particular significance are strong ionic contacts. These interactions are known to be crucial for stabilizing the fibroin–chitosan complexes [108]. As shown in Figure 3, in the case of both complexes, containing acetic acid and HPO_4^{2-}/Ca^{2+} ions various ionic contacts between chitosan and fibroin appear. However, a significantly higher number of these interactions are observed under the influence of HPO_4^{2-}/Ca^{2+} ions compared to the acetic acid solution. Similarly, Figure 4 reveals a greater frequency of hydrogen bonds between fibroin and chitosan in the presence of HPO_4^{2-} and Ca^{2+} ions. Notably, hydrogen bonds and electrostatic interactions in fibroin blends containing different polysaccharides including chitosan were analyzed using experimental tools [108]. As

indicated by these studies, interactions between the protein and polysaccharides can indeed modify the protein structure itself. From the perspective of bone regeneration, it seems to be beneficial to utilize materials that are structurally similar to natural bone tissue. Fibroin emerges as a promising candidate in this context. It is well established that the crystal phase formed during bone mineralization exhibits a characteristic inter-crystalline center spacing of 0.362 nm [109]. Fortunately, this spacing aligns with the β-sheet conformation observed in fibroin [17]. According to the results of infrared spectroscopy measurements, the complexation of fibroin with chitosan favors the β-sheet conformation of the peptide [108,110,111]. The β-sheet order was also found in the case of the complexes optimized in this study, as visualized by the red band (Figure 2). As inferred from Figures 3 and 4, the contribution of the ionic contacts and hydrogen bond between chitosan and β-sheet fragments is quite significant compared to the contacts formed by other fragments of the peptide (coil, turn). Furthermore, these interactions involve diverse positions in the primary structure of peptide. The effective arrangement of the chitosan chains with respect to the fibroin fragments characterized by the β-sheet order is shown in Figure 2.

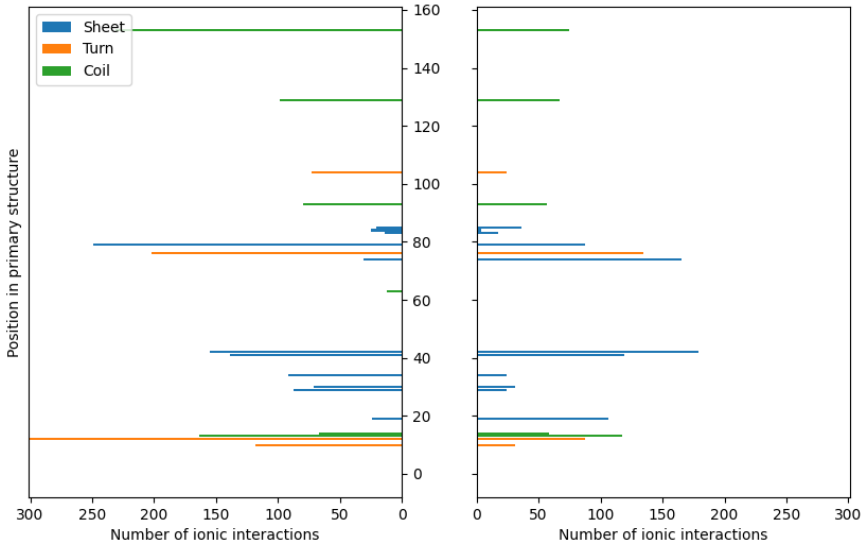

Figure 3. The distributions of ionic contacts in the case of fibroin–chitosan complexes stabilized by HPO_4^{2-}/Ca^{2+} (**left panel**) and acetic acid aqueous solution (**right panel**).

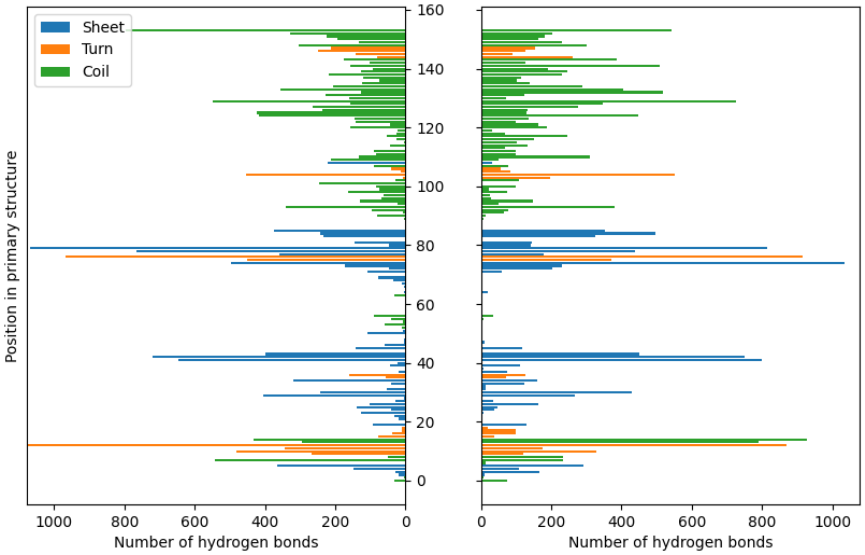

Figure 4. The distributions of hydrogen bonds in the case of fibroin–chitosan complexes stabilized by HPO_4^{2-}/Ca^{2+} (**left panel**) and acetic acid aqueous solution (**right panel**).

The visualization of all main types of interactions formed in the considered systems (ionic contacts, hydrophobic contacts and hydrogen bonds) was presented in Figures 5 and 6. The optimized structures of fibroin–chitosan complexes are stabilized by strong hydrogen bonds and ionic interactions, which are characterized by short interatomic distances ranging from 1.85 to 2.11 Å for hydrogen bonds and from 3.83 to 3.92 Å for ionic contacts. The latter type of interactions deserve special attention due to their diversity and the direct involvement of the ions added to the fibroin–chitosan system considered in this study. As established, Ca^{2+} and HPO_4^{2-} ions facilitate the formation of ionic bridges. The bridges involving HPO_4^{2-} were formed through interactions between protonated amino groups in chitosan and lysine (LYS) residues within the fibroin (Figure 6). Interestingly, no analogous interactions were detected in the case of systems containing CH_3COO^- ions. In this study, fully deacetylated chitosan was used. It is worth mentioning that previous studies [61,62] have shown that a degree of chitosan deacetylation enhances the stability of collagen–chitosan complexes. This underscores the importance of the presence of protonated amino groups in stabilizing the system, as can be observed by analyzing key hydrogen bonds (Figure 5) and ionic interactions (Figure 6). Of course, the impact of deacetylation on the affinity of chitosan for fibroin requires further investigation. Another interesting aspect to explore is the ratio of fibroin to chitosan. In this study, a relatively large number of fibroin chains were used compared to chitosan, allowing for extensive involvement of chitosan in molecular contacts, as seen in Figure 2. Notably, in the case of composites containing fibroin, chitosan, and nanohydroxyapatite, increasing the proportion of fibroin is advantageous for the development of osteogenic cells [87].

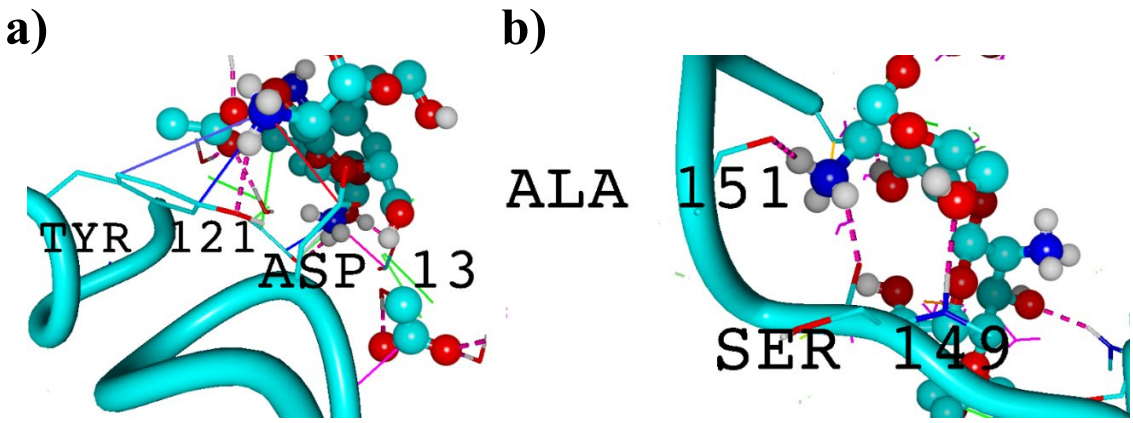

Figure 5. Visualization of silk fibroin helices interacting with chitosan in the presence of acetic acid. Hydrogen bonds are denoted by pink dotted lines, while ionic contacts are denoted by solid red lines. Solid green lines stand for hydrophobic contacts and solid blue pi-stacking. Fibroin helices are presented as solid turquoise lines, whereas chitosan is represented by a ball–stick model with colors representing the following elements: carbon—turquoise, nitrogen—dark blue, phosphorus—yellow, oxygen—red, and hydrogen—white. (**a**) shows interactions involving tyrosine (TYR) and aspartic acid (ASP) residues, while (**b**) illustrates interactions involving alanine (ALA) and serine (SER) residues.

The analysis of molecular contacts involving Ca^{2+} seems to offer valuable insights into the stabilization of potential biomaterials used for bone regeneration. It is well known that the addition of calcium salts is advantageous for the solubilization of fibroin [17], indicating Ca^{2+}/peptide interactions. When considering the impact of Ca^{2+} ions on the peptide structure, it is important to note that they can strongly interact with fibroin, leading to a reduction in the number of β-sheet domains [112]. This, in turn, affects the mechanical properties of the material. Notably, an experimental study by Koeppel et al. [113] confirms that the carboxylic groups in ASP and GLU in silk peptides form ionic contacts with Ca^{2+} and K^+, which has a significant impact on their rheological properties. However, the presence of chitosan has a beneficial effect on β-sheet formation [67,111,114],

which probably compensates the effect of Ca^{2+} ions. As expected, in light of the this research, the interactions with Ca^{2+} can be observed in the regions characterized by β-sheet conformation (Figure 6c,d). Structural details of the identified ionic bridges (ASP-Ca^{2+}-ASP, ASP-Ca^{2+}-GLU, ASP-Ca^{2+}-GLY, GLU-Ca^{2+}-GLU, GLU-Ca^{2+}-GLY) are provided in Supplementary Table S3.

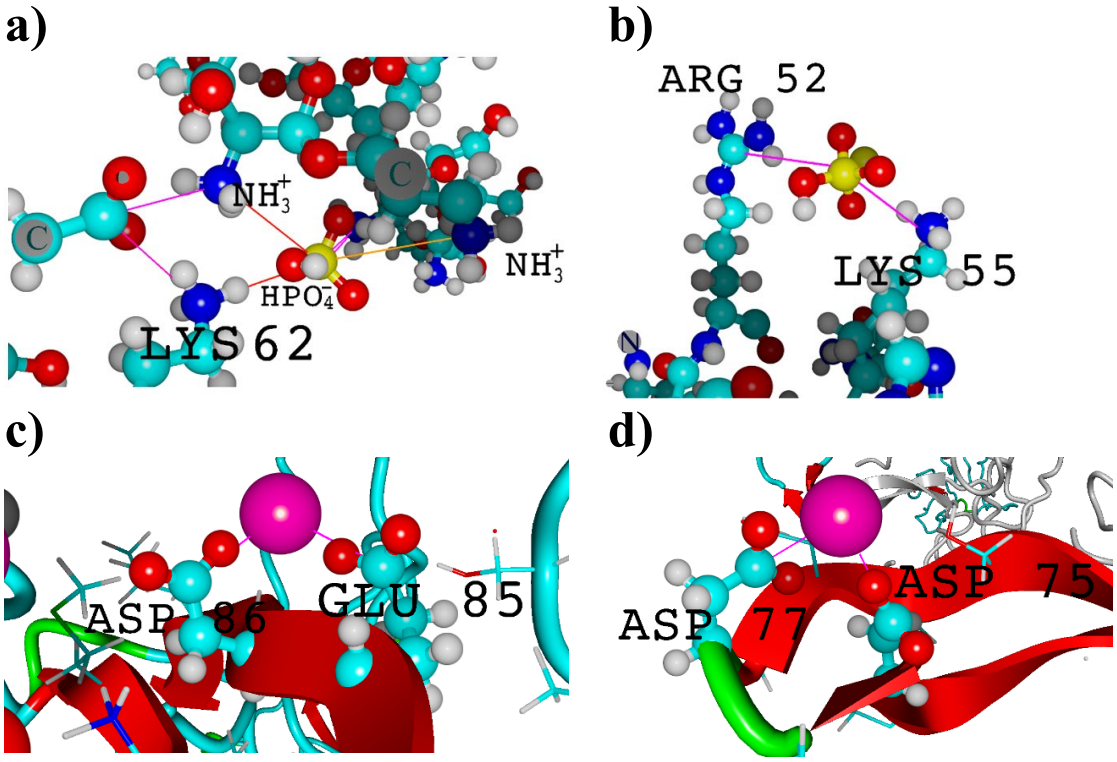

Figure 6. Visualization of (**a**) intermolecular fibroin ion bridges with chitosan carried by phosphoric ions; (**b**) intramolecular arginine–lysine ion bridge; (**c**,**d**) calcium ion-mediated ion bridges. Molecules are represented by a ball–stick model with colors representing the following elements: carbon—turquoise, nitrogen—dark blue, phosphorus—yellow, oxygen—red and hydrogen—white, calcium—pink.

To identify hydrogen bonds, a default YASARA protocol based on an energy calculation with a specified threshold of −6.25 kJ/mol was applied [115]. The molecular dynamics simulations revealed that ALA, ARG, ASN, ASP, GLN, GLU, GLY, LEU, PRO, SER, THR, TYR, and VAL form the strongest hydrogen bonds, whether the complexes are stabilized by CH_3COOH or $Ca^{2+}/HPO_4{}^{2-}$. The highest binding energy values were observed in the case of ARG, reaching 22.30 ± 3.45 kJ/mol for acetic-acid-stabilized complexes and 19.49 ± 5.86 kJ/mol for systems stabilized by Ca^{2+} and $HPO_4{}^{2-}$ ions. Among these hydrogen bonds, interactions formed by ASP were found to be the most significant contributors, constituting approximately 26.3% of all hydrogen bonding interactions. A considerable contribution to complex stabilization was also noted for SER residues. In the case of complexes stabilized by acetic acid, hydrogen bonds involving SER exhibited a binding energy of 18.16 ± 5.45 kJ/mol, accounting for 10.5% of all hydrogen bonds, while those stabilized by Ca^{2+} and $HPO_4{}^{2-}$ ions accounted for 10% (18.36 ± 5.56 kJ/mol). Additionally, THR residues were observed to form relatively strong hydrogen bonds, with binding energies of 17.72 ± 5.91 kJ/mol (CH_3COOH) and 18.80 ± 5.60 kJ/mol ($Ca^{2+}/HPO_4{}^{2-}$). Notably, both SER and THR play an important structural role in silk fibroin. Since SER and THR residues contain active hydroxyl groups, they serve as attachment sites for carbohydrates. Furthermore, SER serves as the phosphorylation site [21]. In hydrogen bonding, SER and THR can act as both hydrogen donors and acceptors. Moreover, SER is often found in tight bends or loops, faces outward, forming hydrogen bonds with molecules of the

medium (water) [21]. THR residue, which is more hydrophobic than SER, often occurs in an antiparallel β-sheet, facing the inside of the molecule [21].

Unlike ionic interactions and hydrogen bonds, hydrophobic contacts exhibit less significant differences in distribution between complexes stabilized by HPO_4^{2-}/Ca^{2+} and acetic acid (Figure 7). Nevertheless, their contribution to complex stabilization is much less important compared to previously discussed short-distance interactions. According to the applied default criteria [115] used for the detection of hydrophobic contacts in the YASARA software (2021), this type of weak contact involves carbon atoms surrounded by three or two hydrogen or carbon atoms, or C-H moieties in carbon rings [116]. As expected, the majority of hydrophobic contacts are formed by aromatic residues in the fibroin chain (PHE and TYR, Supplementary Table S4). The interatomic distances determined for these interactions range from 4.33 to 4.54 Å (CH_3COOH) and from 4.25 to 4.66 Å (Ca^{2+}/HPO_4^{2-}).

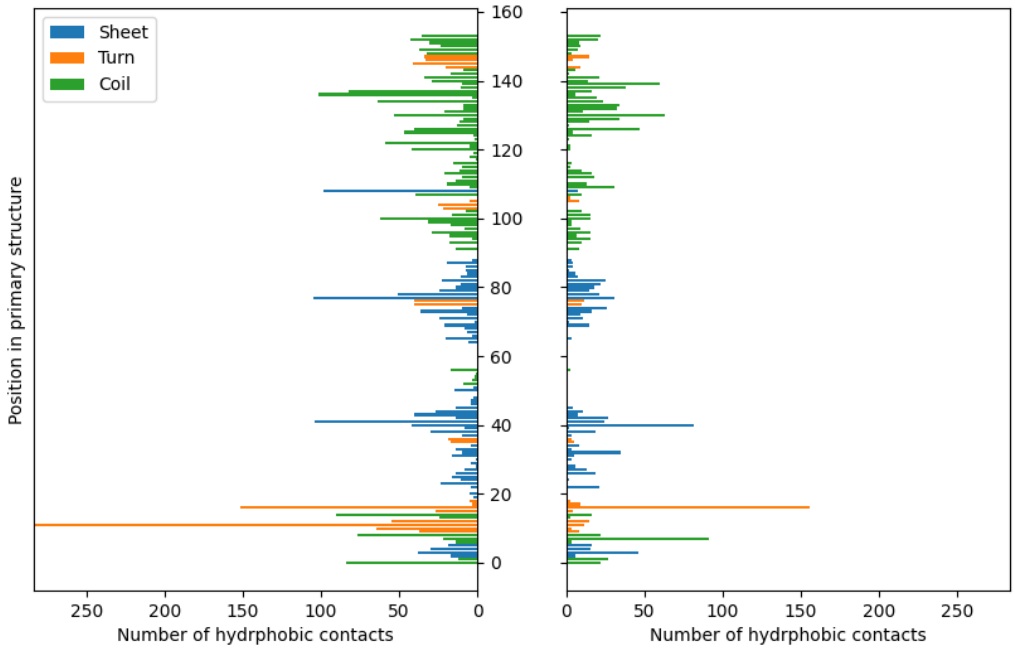

Figure 7. The distributions of hydrophobic contacts in the case of fibroin–chitosan complexes stabilized by HPO_4^{2-}/Ca^{2+} (**left panel**) and acetic acid aqueous solution (**right panel**).

It is worth noting that, in addition to the aforementioned main types of interactions, a relatively weak but identifiable cation-π contact can also be distinguished. The distances determined for these contacts are relatively large and range from 3.80 to 4.19 Å (in the case of the complexes containing Ca^{2+} and HPO_4^{2-}) and from 3.91 to 4.23 Å (in the case of the complexes containing CH_3COOH). These interactions involve the positively charged ammonium group in chitosan and the moieties in fibroin, containing π electrons. Our analysis reveals that HPO_4^{2-}/Ca^{2+}-influenced complexes involve cation-π contacts formed by HIS (11.0%), PHE (39.3%), and TYR (49.7%). Interestingly, complexes formed with CH_3COOH exhibit interactions with a wider range of residues, including ASP (7.0%), GLU (4.1%), GLY (0.2%), HIS (4.3%), PHE (27.3%), and TYR (57.1%).

4. Conclusions

The study focused on the intermolecular interactions in fibroin–chitosan complexes in the presence of Ca^{2+} and HPO_4^{2-} ions, which simulate nanohydroxyapatite, and in the presence of acetic acid. As we found, molecular dynamics simulations performed using the YASARA program revealed a chemically intuitive description of the structural features and interactions between the studied biomolecules. Our analysis showed that the formation of fibroin–chitosan complexes are highly energetically favorable. Furthermore, these systems are much more stable than the previously studied chitosan–collagen complexes. In order to

explain the exceptionally high affinity of fibroin for chitosan, the distributions and structural features of the key interaction types were analyzed. All molecular systems considered in this study were found to have a dense network of intermolecular contacts. Additionally, the optimized structural analysis indicated that the complexation of fibroin with chitosan maintains the β-sheet conformation. Although the obtained results were found to be consistent with various empirical observations, additional experimental studies could provide further confirmation and refinement of the structural and energetical features determined in this study. Molecular dynamics simulations of biomolecule pairs offer valuable insights into the properties of new materials. The promising results obtained for fibroin–chitosan complexes in the presence of $Ca^{2+}/HPO_4{}^{2-}$ and acetic acid suggest the need for further research on the effects of other ions or molecules. These studies could lead to the development of novel fibroin composites with tailored properties for a variety of applications, such as bone regeneration, dentistry and wound dressings.

Supplementary Materials: The following supporting information can be downloaded at: https://www.mdpi.com/article/10.3390/app14104131/s1, Figure S1: Left: RMSD off all atoms evolution (RMSDALL parameter) in time for both cases. Right: the radius gyration analysis of the silk fibroin–chitosan complexes in the presence of $HPO_4{}^{2-}$ and calcium ions (HPO) and acetic acid aqueous solution (Acetic); Figure S2: The frequency of particular types of interactions appearance during MD simulations; Table S1: Description of H-bonds between chitosan and silk fibroins' amino acids along with binding energy values per silk fibroin molecule for both cases; Table S2: Description of ionic interactions between chitosan and silk fibroins' amino acids; Table S3: Distances between groups carried by ion bridges; Table S4: Description of hydrophobic (HP) interactions between chitosan and silk fibroins' amino acids; Table S5: Description of CationPi interactions between chitosan and silk fibroins' amino acids.

Author Contributions: Conceptualization, A.T. and P.B.; methodology, P.B.; software, P.B.; validation, M.P., I.B. and P.B.; formal analysis, M.P., A.T., S.Ś. and P.B.; investigation, M.P. and P.B.; resources, D.L. and P.B.; data curation, P.B.; writing—original draft preparation, M.P., A.T., D.L., S.Ś., A.S., I.B. and P.B.; writing—review and editing, M.P., A.T., D.L., S.Ś., A.S., I.B. and P.B.; visualization, D.L. and P.B.; supervision, A.S.; project administration, M.P. and A.S. All authors have read and agreed to the published version of the manuscript.

Funding: This research received no external funding.

Institutional Review Board Statement: Not applicable.

Informed Consent Statement: Not applicable.

Data Availability Statement: The raw/processed data required to reproduce these findings are available on request.

Conflicts of Interest: Author Iwona Białas was employed by the company CosmetoSAFE Consulting LLC. The remaining authors declare that the research was conducted in the absence of any commercial or financial relationships that could be construed as a potential conflict of interest.

References

1. Mohan, T.; Kleinschek, K.S.; Kargl, R. Polysaccharide peptide conjugates: Chemistry, properties and applications. *Carbohydr. Polym.* **2022**, *280*, 118875. [CrossRef]
2. Song, H.Q.; Fan, Y.; Hu, Y.; Cheng, G.; Xu, F.J. Polysaccharide–Peptide Conjugates: A Versatile Material Platform for Biomedical Applications. *Adv. Funct. Mater.* **2021**, *31*, 2005978. [CrossRef]
3. Sionkowska, A. Collagen blended with natural polymers: Recent advances and trends. *Prog. Polym. Sci.* **2021**, *122*, 101452. [CrossRef]
4. Pomin, V.; Mulloy, B. Glycosaminoglycans and Proteoglycans. *Pharmaceuticals* **2018**, *11*, 27. [CrossRef]
5. Altman, G.H.; Diaz, F.; Jakuba, C.; Calabro, T.; Horan, R.L.; Chen, J.; Lu, H.; Richmond, J.; Kaplan, D.L. Silk-based biomaterials. *Biomaterials* **2003**, *24*, 401–416. [CrossRef] [PubMed]
6. Chen, X.; Qi, Y.-Y.; Wang, L.-L.; Yin, Z.; Yin, G.-L.; Zou, X.-H.; Ouyang, H.-W. Ligament regeneration using a knitted silk scaffold combined with collagen matrix. *Biomaterials* **2008**, *29*, 3683–3692. [CrossRef] [PubMed]
7. Wang, Y.; Kim, H.J.; Vunjak-Novakovic, G.; Kaplan, D.L. Stem cell-based tissue engineering with silk biomaterials. *Biomaterials* **2006**, *27*, 6064–6082. [CrossRef]

8. Shao, Z.; Young, R.J.; Vollrath, F. The effect of solvents on spider silk studied by mechanical testing and single-fibre Raman spectroscopy. *Int. J. Biol. Macromol.* **1999**, *24*, 295–300. [CrossRef]
9. Yang, Y.; Chen, X.; Shao, Z.; Zhou, P.; Porter, D.; Knight, D.P.; Vollrath, F. Toughness of spider silk at high and low temperatures. *Adv. Mater.* **2005**, *17*, 84–88. [CrossRef]
10. Hakimi, O.; Knight, D.P.; Vollrath, F.; Vadgama, P. Spider and mulberry silkworm silks as compatible biomaterials. *Compos. Part B Eng.* **2007**, *38*, 324–337. [CrossRef]
11. Kaplan, D.; Adams, W.W.; Farmer, B.; Viney, C. Silk: Biology, Structure, Properties, and Genetics. In *Silk Polymers*; ACS Symposium Series; American Chemical Society: Washington, DC, USA, 1993; Volume 544, pp. 1–2. ISBN 9780841227439.
12. Finch, C.A. Industrial polymers handbook: Products, Processes, Applications Volume 1, Polymerization processes: Synthetic polymers Volume 2, Synthetic polymers (continued) Volume 3, Synthetic polymers (continued); biopolymers and their derivatives Volume 4, Biopolyme. *Polym. Int.* **2002**, *51*, 264–265.
13. Vollrath, F.; Holtet, T.; Thogersen, H.C.; Frische, S. Structural organization of spider silk. *Proc. R. Soc. B Biol. Sci.* **1996**, *263*, 147–151.
14. Zeng, S.; Ye, M.; Qiu, J.; Fang, W.; Rong, M.; Guo, Z.; Gao, W. Preparation and characterization of genipin-cross-linked silk fibroin/chitosan sustained-release microspheres. *Drug Des. Devel. Ther.* **2015**, *9*, 2501–2514. [CrossRef] [PubMed]
15. Kopp, A.; Smeets, R.; Gosau, M.; Friedrich, R.E.; Fuest, S.; Behbahani, M.; Barbeck, M.; Rutkowski, R.; Burg, S.; Kluwe, L.; et al. Production and characterization of porous fibroin scaffolds for regenerative medical application. *In Vivo* **2019**, *33*, 757–762. [CrossRef] [PubMed]
16. Lee, H.; Park, S.J.; Lee, M.E.; Choi, K.M.; Choi, H.Y.; Hasegawa, Y.; Kim, M.; Kim, K.B. Fabrication of nanofibers using fibroin regenerated by recycling waste silk selvage. *Polym. Bull.* **2020**, *77*, 3853–3862. [CrossRef]
17. Sashina, E.S.; Bochek, A.M.; Novoselov, N.P.; Kirichenko, D.A. Structure and solubility of natural silk fibroin. *Russ. J. Appl. Chem.* **2006**, *79*, 869–876. [CrossRef]
18. Murphy, A.R.; Kaplan, D.L. Biomedical applications of chemically-modified silk fibroin. *J. Mater. Chem.* **2009**, *19*, 6443–6450. [CrossRef]
19. Gauza-Włodarczyk, M.; Kubisz, L.; Włodarczyk, D. Amino acid composition in determination of collagen origin and assessment of physical factors effects. *Int. J. Biol. Macromol.* **2017**, *104*, 987–991. [CrossRef]
20. Patel, M.; Dubey, D.K.; Singh, S.P. Phenomenological models of Bombyx mori silk fibroin and their mechanical behavior using molecular dynamics simulations. *Mater. Sci. Eng. C* **2020**, *108*, 110414. [CrossRef] [PubMed]
21. Hendrich, W. *Molekularna Biofizyka Białka*; Atla 2: Wrocław, Poland, 2005.
22. Jenkins, J.E.; Creager, M.S.; Butler, E.B.; Lewis, R.V.; Yarger, J.L.; Holland, G.P. Solid-state NMR evidence for elastin-like β-turn structure in spider dragline silk. *Chem. Commun.* **2010**, *46*, 6714–6716. [CrossRef] [PubMed]
23. Cheng, Y.; Koh, L.D.; Li, D.; Ji, B.; Han, M.Y.; Zhang, Y.W. On the strength of β-sheet crystallites of Bombyx mori silk fibroin. *J. R. Soc. Interface* **2014**, *11*, 20140305. [CrossRef] [PubMed]
24. Li, X.G.; Wu, L.Y.; Huang, M.R.; Shao, H.L.; Hu, X.C. Conformational transition and liquid crystalline state of regenerated silk fibroin in water. *Biopolymers* **2008**, *89*, 497–505. [CrossRef]
25. Magoshi, J.; Magoshi, Y.; Becker, M.A.; Kato, M.; Han, Z.; Tanaka, T.; Inoue, S.I.; Nakamura, S. Crystallization of silk fibroin from solution. *Thermochim. Acta* **2000**, *352*, 165–169. [CrossRef]
26. He, S.J.; Valluzzi, R.; Gido, S.P. Silk I structure in Bombyx mori silk foams. *Int. J. Biol. Macromol.* **1999**, *24*, 187–195. [CrossRef] [PubMed]
27. Jin, H.J.; Kaplan, D.L. Mechanism of silk processing in insects and spiders. *Nature* **2003**, *424*, 1057–1061. [CrossRef] [PubMed]
28. Farokhi, M.; Mottaghitalab, F.; Reis, R.L.; Ramakrishna, S.; Kundu, S.C. Functionalized silk fibroin nanofibers as drug carriers: Advantages and challenges. *J. Control Release* **2020**, *321*, 324–347. [CrossRef] [PubMed]
29. Wenk, E.; Merkle, H.P.; Meinel, L. Silk fibroin as a vehicle for drug delivery applications. *J. Control Release* **2011**, *150*, 128–141. [CrossRef] [PubMed]
30. Opriș, O.; Mormile, C.; Lung, I.; Stegarescu, A.; Soran, M.-L.; Soran, A. An Overview of Biopolymers for Drug Delivery Applications. *Appl. Sci.* **2024**, *14*, 1383. [CrossRef]
31. Khosravimelal, S.; Mobaraki, M.; Eftekhari, S.; Ahearne, M.; Seifalian, A.M.; Gholipourmalekabadi, M. Hydrogels as Emerging Materials for Cornea Wound Healing. *Small* **2021**, *17*, 2006335. [CrossRef]
32. Zhou, H.; Wang, Z.; Cao, H.; Hu, H.; Luo, Z.; Yang, X.; Cui, M.; Zhou, L. Genipin-crosslinked polyvinyl alcohol/silk fibroin/nano-hydroxyapatite hydrogel for fabrication of artificial cornea scaffolds—A novel approach to corneal tissue engineering. *J. Biomater. Sci. Polym. Ed.* **2019**, *30*, 1604–1619. [CrossRef]
33. Grabska-Zielińska, S.; Sionkowska, A. How to improve physico-chemical properties of silk fibroin materials for biomedical applications?—Blending and cross-linking of silk fibroin—A review. *Materials* **2021**, *14*, 1510. [CrossRef] [PubMed]
34. Tuwalska, A.; Grabska-Zielińska, S.; Sionkowska, A. Chitosan/Silk Fibroin Materials for Biomedical Applications—A Review. *Polymers* **2022**, *14*, 1343. [CrossRef] [PubMed]
35. Azmana, M.; Mahmood, S.; Hilles, A.R.; Rahman, A.; Arifin, M.A.B.; Ahmed, S. A review on chitosan and chitosan-based bionanocomposites: Promising material for combatting global issues and its applications. *Int. J. Biol. Macromol.* **2021**, *185*, 832–848. [CrossRef] [PubMed]

36. Picos-Corrales, L.A.; Morales-Burgos, A.M.; Ruelas-Leyva, J.P.; Crini, G.; García-Armenta, E.; Jimenez-Lam, S.A.; Ayón-Reyna, L.E.; Rocha-Alonzo, F.; Calderón-Zamora, L.; Osuna-Martínez, U.; et al. Chitosan as an Outstanding Polysaccharide Improving Health-Commodities of Humans and Environmental Protection. *Polymers* **2023**, *15*, 526. [CrossRef]
37. Morin-Crini, N.; Lichtfouse, E.; Torri, G.; Crini, G. Applications of chitosan in food, pharmaceuticals, medicine, cosmetics, agriculture, textiles, pulp and paper, biotechnology, and environmental chemistry. *Environ. Chem. Lett.* **2019**, *17*, 1667–1692. [CrossRef]
38. Riseh, R.S.; Vazvani, M.G.; Kennedy, J.F. The application of chitosan as a carrier for fertilizer: A review. *Int. J. Biol. Macromol.* **2023**, *252*, 126483. [CrossRef] [PubMed]
39. Kumar, M.N.V.R.; Muzzarelli, R.A.A.; Muzzarelli, C.; Sashiwa, H.; Domb, A.J. Chitosan Chemistry and Pharmaceutical Perspectives. *Chem. Rev.* **2004**, *104*, 6017–6084. [CrossRef] [PubMed]
40. Li, X.; Zhang, X.; Zhao, W.; Tian, P.; Tulugan, K. Preparation of Hirudin-Loaded Chitosan/Polycaprolactone Bowl-Shaped Particles and an Application for a Drug Delivery System. *Appl. Sci.* **2024**, *14*, 1939. [CrossRef]
41. Manna, S.; Seth, A.; Gupta, P.; Nandi, G.; Dutta, R.; Jana, S.; Jana, S. Chitosan Derivatives as Carriers for Drug Delivery and Biomedical Applications. *ACS Biomater. Sci. Eng.* **2023**, *9*, 2181–2202. [CrossRef]
42. Desai, N.; Rana, D.; Salave, S.; Gupta, R.; Patel, P.; Karunakaran, B.; Sharma, A.; Giri, J.; Benival, D.; Kommineni, N. Chitosan: A Potential Biopolymer in Drug Delivery and Biomedical Applications. *Pharmaceutics* **2023**, *15*, 1313. [CrossRef]
43. Budiarso, I.J.; Rini, N.D.W.; Tsalsabila, A.; Birowosuto, M.D.; Wibowo, A. Chitosan-Based Smart Biomaterials for Biomedical Applications: Progress and Perspectives. *ACS Biomater. Sci. Eng.* **2023**, *9*, 3084–3115. [CrossRef] [PubMed]
44. Manigandan, V.; Karthik, R.; Ramachandran, S.; Rajagopal, S. Chitosan Applications in Food Industry. In *Biopolymers for Food Design*; Elsevier: Amsterdam, The Netherlands, 2018; pp. 469–491.
45. Li, J.; Tian, X.; Hua, T.; Fu, J.; Koo, M.; Chan, W.; Poon, T. Chitosan Natural Polymer Material for Improving Antibacterial Properties of Textiles. *ACS Appl. Bio Mater.* **2021**, *4*, 4014–4038. [CrossRef] [PubMed]
46. Klinkhammer, K.; Hohenbild, H.; Hoque, M.T.; Elze, L.; Teshay, H.; Mahltig, B. Functionalization of Technical Textiles with Chitosan. *Textiles* **2024**, *4*, 70–90. [CrossRef]
47. Riaz Rajoka, M.S.; Zhao, L.; Mehwish, H.M.; Wu, Y.; Mahmood, S. Chitosan and its derivatives: Synthesis, biotechnological applications, and future challenges. *Appl. Microbiol. Biotechnol.* **2019**, *103*, 1557–1571. [CrossRef] [PubMed]
48. Kulka, K.; Sionkowska, A. Chitosan Based Materials in Cosmetic Applications: A Review. *Molecules* **2023**, *28*, 1817. [CrossRef] [PubMed]
49. Aranaz, I.; Acosta, N.; Civera, C.; Elorza, B.; Mingo, J.; Castro, C.; Gandía, M.; Heras Caballero, A. Cosmetics and Cosmeceutical Applications of Chitin, Chitosan and Their Derivatives. *Polymers* **2018**, *10*, 213. [CrossRef]
50. Guzmán, E.; Ortega, F.; Rubio, R.G. Chitosan: A Promising Multifunctional Cosmetic Ingredient for Skin and Hair Care. *Cosmetics* **2022**, *9*, 99. [CrossRef]
51. Sionkowska, A.; Lewandowska, K.; Kurzawa, M. Chitosan-Based Films Containing Rutin for Potential Cosmetic Applications. *Polymers* **2023**, *15*, 3224. [CrossRef] [PubMed]
52. Gal, M.R.; Rahmaninia, M.; Hubbe, M.A. A comprehensive review of chitosan applications in paper science and technologies. *Carbohydr. Polym.* **2023**, *309*, 120665. [CrossRef]
53. Bakshi, P.S.; Selvakumar, D.; Kadirvelu, K.; Kumar, N.S. Chitosan as an environment friendly biomaterial—A review on recent modifications and applications. *Int. J. Biol. Macromol.* **2020**, *150*, 1072–1083. [CrossRef]
54. Shi, S.; Liu, X.; Li, W.; Li, Z.; Tu, G.; Deng, B.; Liu, C. Tuning the Biodegradability of Chitosan Membranes: Characterization and Conceptual Design. *ACS Sustain. Chem. Eng.* **2020**, *8*, 14484–14492. [CrossRef]
55. Chang, X.X.; Mubarak, N.M.; Ali Mazari, S.; Sattar Jatoi, A.; Ahmad, A.; Khalid, M.; Walvekar, R.; Abdullah, E.C.; Karri, R.R.; Siddiqui, M.T.; et al. A review on the properties and applications of chitosan, cellulose and deep eutectic solvent in green chemistry. *J. Ind. Eng. Chem.* **2021**, *104*, 362–380. [CrossRef]
56. Haugh, M.G.; Jaasma, M.J.; O'Brien, F.J. The effect of dehydrothermal treatment on the mechanical and structural properties of collagen-GAG scaffolds. *J. Biomed. Mater. Res. Part A* **2009**, *89*, 363–369. [CrossRef]
57. Rohanizadeh, R.; Kokabi, N. Heat denatured/aggregated albumin-based biomaterial: Effects of preparation parameters on biodegradability and mechanical properties. *J. Mater. Sci. Mater. Med.* **2009**, *20*, 2413–2418. [CrossRef] [PubMed]
58. Lei, Y.; Gao, S.; Xiang, X.; Li, X.; Yu, X.; Li, S. Physicochemical, structural and adhesion properties of walnut protein isolate-xanthan gum composite adhesives using walnut protein modified by ethanol. *Int. J. Biol. Macromol.* **2021**, *192*, 644–653. [CrossRef]
59. Ozden, E.; Atilgan, A.R.; Bilge, K.; Menceloglu, Y.Z.; Atılgan, C.; Papila, M. Designed-in Molecular Interactions Lead to Superior Thermo-mechanical Properties in Nanocomposites. *MRS Proc.* **2011**, *1304*, mrsf10-1304-z09-10. [CrossRef]
60. Sun, X.; Xu, G.; Zhang, J.; Xu, Y. Effects of interface cohesion on mechanical properties of interpenetrating phase nanocomposites. *Micro Nano Lett.* **2014**, *9*, 697–701. [CrossRef]
61. Bełdowski, P.; Przybyłek, M.; Sionkowska, A.; Cysewski, P.; Gadomska, M.; Musiał, K.; Gadomski, A. Effect of Chitosan Deacetylation on Its Affinity to Type III Collagen: A Molecular Dynamics Study. *Materials* **2022**, *15*, 463. [CrossRef] [PubMed]
62. Przybyłek, M.; Bełdowski, P.; Wieland, F.; Cysewski, P.; Sionkowska, A. Collagen Type II—Chitosan Interactions as Dependent on Hydroxylation and Acetylation Inferred from Molecular Dynamics Simulations. *Molecules* **2022**, *28*, 154. [CrossRef]
63. Przybyłek, M.; Bełdowski, P. Molecular dynamics simulations of the affinity of chitin and chitosan for collagen: The effect of ph and the presence of sodium and calcium cations. *Prog. Chem. Appl. Chitin Its Deriv.* **2023**, *28*, 136–150. [CrossRef]

64. Bełdowski, P.; Przybyłek, M.; Bełdowski, D.; Dedinaite, A.; Sionkowska, A.; Cysewski, P.; Claesson, P.M. Collagen type II–hyaluronan interactions—The effect of proline hydroxylation: A molecular dynamics study. *J. Mater. Chem. B* **2022**, *10*, 9713–9723. [CrossRef] [PubMed]
65. Muzzarelli, R.A.A.; Greco, F.; Busilacchi, A.; Sollazzo, V.; Gigante, A. Chitosan, hyaluronan and chondroitin sulfate in tissue engineering for cartilage regeneration: A review. *Carbohydr. Polym.* **2012**, *89*, 723–739. [CrossRef] [PubMed]
66. Kim, H.S.; Kim, J.T.; Jung, Y.J.; Ryu, S.C.; Son, H.J.; Kim, Y.G. Preparation of a porous chitosan/fibroin-hydroxyapatite composite matrix for tissue engineering. *Macromol. Res.* **2007**, *15*, 65–73. [CrossRef]
67. Luangbudnark, W.; Viyoch, J.; Laupattarakasem, W.; Surakunprapha, P.; Laupattarakasem, P. Properties and biocompatibility of chitosan and silk fibroin blend films for application in skin tissue engineering. *Sci. World J.* **2012**, *2012*, 1–10. [CrossRef] [PubMed]
68. Fernandez, J.G.; Ingber, D.E. Unexpected Strength and Toughness in Chitosan-Fibroin Laminates Inspired by Insect Cuticle. *Adv. Mater.* **2012**, *24*, 480–484. [CrossRef]
69. Li, J.; Wang, Q.; Gu, Y.; Zhu, Y.; Chen, L.; Chen, Y. Production of Composite Scaffold Containing Silk Fibroin, Chitosan, and Gelatin for 3D Cell Culture and Bone Tissue Regeneration. *Med. Sci. Monit.* **2017**, *23*, 5311–5320. [CrossRef] [PubMed]
70. Xu, Z.; Chen, T.; Zhang, K.; Meng, K.; Zhao, H. Silk fibroin/chitosan hydrogel with antibacterial, hemostatic and sustained drug-release activities. *Polym. Int.* **2021**, *70*, 1741–1751. [CrossRef]
71. Ducret, M.; Montembault, A.; Josse, J.; Pasdeloup, M.; Celle, A.; Benchrih, R.; Mallein-Gerin, F.; Alliot-Licht, B.; David, L.; Farges, J.-C. Design and characterization of a chitosan-enriched fibrin hydrogel for human dental pulp regeneration. *Dent. Mater.* **2019**, *35*, 523–533. [CrossRef] [PubMed]
72. Aguilar, A.; Zein, N.; Harmouch, E.; Hafdi, B.; Bornert, F.; Offner, D.; Clauss, F.; Fioretti, F.; Huck, O.; Benkirane-Jessel, N.; et al. Application of Chitosan in Bone and Dental Engineering. *Molecules* **2019**, *24*, 3009. [CrossRef]
73. Dorozhkin, S.V. There Are over 60 Ways to Produce Biocompatible Calcium Orthophosphate ($CaPO_4$) Deposits on Various Substrates. *J. Compos. Sci.* **2023**, *7*, 273. [CrossRef]
74. Zafar, M.S.; Al-Samadani, K.H. Potential use of natural silk for bio-dental applications. *J. Taibah Univ. Med. Sci.* **2014**, *9*, 171–177. [CrossRef]
75. Alsalhi, A. Applications of selected polysaccharides and proteins in dentistry: A review. *Int. J. Biol. Macromol.* **2024**, *260*, 129215. [CrossRef] [PubMed]
76. Min, Q.; Tian, D.; Zhang, Y.; Wang, C.; Wan, Y.; Wu, J. Strong and Elastic Chitosan/Silk Fibroin Hydrogels Incorporated with Growth-Factor-Loaded Microspheres for Cartilage Tissue Engineering. *Biomimetics* **2022**, *7*, 41. [CrossRef]
77. Van der Elst, M.; Klein, C.P.A.T.; de Blieck-Hogervorst, J.M.; Patka, P.; Haarman, H.J.T.M. Bone tissue response to biodegradable polymers used for intra medullary fracture fixation: A long-term in vivo study in sheep femora. *Biomaterials* **1999**, *20*, 121–128. [CrossRef] [PubMed]
78. Krieger, E.; Vriend, G. YASARA View—Molecular graphics for all devices—From smartphones to workstations. *Bioinformatics* **2014**, *30*, 2981–2982. [CrossRef] [PubMed]
79. Krieger, E.; Koraimann, G.; Vriend, G. Increasing the precision of comparative models with YASARA NOVA—A self-parameterizing force field. *Proteins Struct. Funct. Genet.* **2002**, *47*, 393–402. [CrossRef] [PubMed]
80. Andrysiak, T.; Bełdowski, P.; Siódmiak, J.; Weber, P.; Ledziński, D. Hyaluronan-Chondroitin Sulfate Anomalous Crosslinking Due to Temperature Changes. *Polymers* **2018**, *10*, 560. [CrossRef] [PubMed]
81. Li, J.; Qin, X.; Liu, X.; Li, J.; Zhong, J. Enhanced mechanical, barrier and antioxidant properties of rice protein/sodium alginate-based films by incorporating cellulose nanocrystals and rosemary extract. *Food Packag. Shelf Life* **2022**, *34*, 101000. [CrossRef]
82. Kulik, N.; Minofar, B.; Jugl, A.; Pekař, M. Computational Study of Complex Formation between Hyaluronan Polymers and Polyarginine Peptides at Various Ratios. *Langmuir* **2023**, *39*, 14212–14222. [CrossRef]
83. Li, D.-W.; He, J.; He, F.-L.; Liu, Y.-L.; Liu, Y.-Y.; Ye, Y.-J.; Deng, X.; Yin, D.-C. Silk fibroin/chitosan thin film promotes osteogenic and adipogenic differentiation of rat bone marrow-derived mesenchymal stem cells. *J. Biomater. Appl.* **2018**, *32*, 1164–1173. [CrossRef]
84. Chen, J.-P.; Chen, S.-H.; Lai, G.-J. Preparation and characterization of biomimetic silk fibroin/chitosan composite nanofibers by electrospinning for osteoblasts culture. *Nanoscale Res. Lett.* **2012**, *7*, 170. [CrossRef] [PubMed]
85. Strobin, G.; Ciechańska, D.; Wawro, D.; Stęplewski, W.; Jóźwicka, J.; Sobczak, S.; Haga, A. Chitosan Fibres Modified by Fibroin. *Fib. Text. East. Eur.* **2007**, *15*, 146–148.
86. De Moraes, M.A.; Nogueira, G.M.; Weska, R.F.; Beppu, M.M. Preparation and Characterization of Insoluble Silk Fibroin/Chitosan Blend Films. *Polymers* **2010**, *2*, 719–727. [CrossRef]
87. Tuwalska, A.; Sionkowska, A.; Bryła, A.; Tylko, G.; Osyczka, A.M.; Laus, M.; Vojtová, L. A Biological Study of Composites Based on the Blends of Nanohydroxyapatite, Silk Fibroin and Chitosan. *Materials* **2022**, *15*, 5444. [CrossRef] [PubMed]
88. Zakharova, V.A.; Kildeeva, N.R. Biopolymer Matrices Based on Chitosan and Fibroin: A Review Focused on Methods for Studying Surface Properties. *Polysaccharides* **2021**, *2*, 154–167. [CrossRef]
89. Duan, Y.; Wu, C.; Chowdhury, S.; Lee, M.C.; Xiong, G.; Zhang, W.; Yang, R.; Cieplak, P.; Luo, R.; Lee, T.; et al. A Point-Charge Force Field for Molecular Mechanics Simulations of Proteins Based on Condensed-Phase Quantum Mechanical Calculations. *J. Comput. Chem.* **2003**, *24*, 1999–2012. [CrossRef] [PubMed]
90. Kirschner, K.N.; Yongye, A.B.; Tschampel, S.M.; González-Outeiriño, J.; Daniels, C.R.; Foley, B.L.; Woods, R.J. GLYCAM06: A generalizable biomolecular force field. carbohydrates. *J. Comput. Chem.* **2008**, *29*, 622–655. [CrossRef] [PubMed]

91. Markwick, P.R.L.; Peacock, R.B.; Komives, E.A. Accurate Prediction of Amide Exchange in the Fast Limit Reveals Thrombin Allostery. *Biophys. J.* **2019**, *116*, 49–56. [CrossRef] [PubMed]
92. Izmailov, S.A.; Podkorytov, I.S.; Skrynnikov, N.R. Simple MD-based model for oxidative folding of peptides and proteins. *Sci. Rep.* **2017**, *7*, 9293. [CrossRef]
93. Childers, M.C.; Daggett, V. Validating Molecular Dynamics Simulations against Experimental Observables in Light of Underlying Conformational Ensembles. *J. Phys. Chem. B* **2018**, *122*, 6673–6689. [CrossRef]
94. Maier, J.A.; Martinez, C.; Kasavajhala, K.; Wickstrom, L.; Hauser, K.E.; Simmerling, C. ff14SB: Improving the Accuracy of Protein Side Chain and Backbone Parameters from ff99SB. *J. Chem. Theory Comput.* **2015**, *11*, 3696–3713. [CrossRef] [PubMed]
95. Salisburg, A.M.; Deline, A.L.; Lexa, K.W.; Shields, G.C.; Kirschner, K.N. Ramachandran-type plots for glycosidic linkages: Examples from molecular dynamic simulations using the Glycam06 force field. *J. Comput. Chem.* **2009**, *30*, 910–921. [CrossRef]
96. Miyamoto, H.; Schnupf, U.; Crowley, M.F.; Brady, J.W. Comparison of the simulations of cellulosic crystals with three carbohydrate force fields. *Carbohydr. Res.* **2016**, *422*, 17–23. [CrossRef]
97. Krieger, E.; Dunbrack, R.L.; Hooft, R.W.W.; Krieger, B. Assignment of protonation states in proteins and ligands: Combining pK a prediction with hydrogen bonding network optimization. *Methods Mol. Biol.* **2012**, *819*, 405–421.
98. Essmann, U.; Perera, L.; Berkowitz, M.L.; Darden, T.; Lee, H.; Pedersen, L.G. A smooth particle mesh Ewald method. *J. Chem. Phys.* **1995**, *103*, 8577–8593. [CrossRef]
99. Berendsen, H.J.C.; Postma, J.P.M.; van Gunsteren, W.F.; DiNola, A.; Haak, J.R. Molecular dynamics with coupling to an external bath. *J. Chem. Phys.* **1984**, *81*, 3684–3690. [CrossRef]
100. Xu, Z.; Tang, E.; Zhao, H. An Environmentally Sensitive Silk Fibroin/Chitosan Hydrogel and Its Drug Release Behaviors. *Polymers* **2019**, *11*, 1980. [CrossRef]
101. Chen, X.; Li, W.; Zhong, W.; Lu, Y.; Yu, T. pH sensitivity and ion sensitivity of hydrogels based on complex-forming chitosan/silk fibroin interpenetrating polymer network. *J. Appl. Polym. Sci.* **1997**, *65*, 2257–2262. [CrossRef]
102. Sashina, E.S.; Janowska, G.; Zaborski, M.; Vnuchkin, A.V. Compatibility of fibroin/chitosan and fibroin/cellulose blends studied by thermal analysis. *J. Therm. Anal. Calorim.* **2007**, *89*, 887–891. [CrossRef]
103. Pham, D.T.; Tiyaboonchai, W. Fibroin nanoparticles: A promising drug delivery system. *Drug Deliv.* **2020**, *27*, 431–448. [CrossRef]
104. Malay, Ö.; Bayraktar, O.; Batigün, A. Complex coacervation of silk fibroin and hyaluronic acid. *Int. J. Biol. Macromol.* **2007**, *40*, 387–393. [CrossRef] [PubMed]
105. Bhardwaj, N.; Kundu, S.C. Silk fibroin protein and chitosan polyelectrolyte complex porous scaffolds for tissue engineering applications. *Carbohydr. Polym.* **2011**, *85*, 325–333. [CrossRef]
106. Malay, Ö.; Batıgün, A.; Bayraktar, O. pH- and electro-responsive characteristics of silk fibroin–hyaluronic acid polyelectrolyte complex membranes. *Int. J. Pharm.* **2009**, *380*, 120–126. [CrossRef] [PubMed]
107. Ghaeli, I.; de Moraes, M.; Beppu, M.; Lewandowska, K.; Sionkowska, A.; Ferreira-da-Silva, F.; Ferraz, M.; Monteiro, F. Phase Behaviour and Miscibility Studies of Collagen/Silk Fibroin Macromolecular System in Dilute Solutions and Solid State. *Molecules* **2017**, *22*, 1368. [CrossRef] [PubMed]
108. Shang, S.; Zhu, L.; Fan, J. Intermolecular interactions between natural polysaccharides and silk fibroin protein. *Carbohydr. Polym.* **2013**, *93*, 561–573. [CrossRef] [PubMed]
109. Pawlikowski, M.; Niedźwiedzki, T. *Mineralogia Kości*; PAN: Cracow, Poland, 2002.
110. Park, S.J.; Lee, K.Y.; Wan Shik, H.A.; Park, S.Y. Structural changes and their effect on mechanical properties of silk fibroin/chitosan blends. *J. Appl. Polym. Sci.* **1999**, *74*, 2571–2575. [CrossRef]
111. Delezuk, J.A.M.; Pavinatto, A.; Moraes, M.L.; Shimizu, F.M.; Rodrigues, V.C.; Campana-Filho, S.P.; Ribeiro, S.J.L.; Oliveira, O.N. Silk fibroin organization induced by chitosan in layer-by-layer films: Application as a matrix in a biosensor. *Carbohydr. Polym.* **2017**, *155*, 146–151. [CrossRef] [PubMed]
112. Drnovšek, N.; Kocen, R.; Gantar, A.; Drobnič-Košorok, M.; Leonardi, A.; Križaj, I.; Rečnik, A.; Novak, S. Size of silk fibroin β-sheet domains affected by Ca^{2+}. *J. Mater. Chem. B* **2016**, *4*, 6597–6608. [CrossRef] [PubMed]
113. Koeppel, A.; Laity, P.R.; Holland, C. The influence of metal ions on native silk rheology. *Acta Biomater.* **2020**, *117*, 204–212. [CrossRef]
114. Chen, X.; Li, W.; Yu, T. Conformation transition of silk fibroin induced by blending chitosan. *J. Polym. Sci. Part B Polym. Phys.* **1997**, *35*, 2293–2296. [CrossRef]
115. Krieger, E.; Vriend, G. New ways to boost molecular dynamics simulations. *J. Comput. Chem.* **2015**, *36*, 996–1007. [CrossRef] [PubMed]
116. Xu, B.; Jacobs, M.I.; Kostko, O.; Ahmed, M. Guanidinium Group Remains Protonated in a Strongly Basic Arginine Solution. *ChemPhysChem* **2017**, *18*, 1503–1506. [CrossRef] [PubMed]